AGU100 ADVANCING EARTH AND SPACE SCIENCE

Water Resources Research

RESEARCH ARTICLE
10.1029/2017WR022279

Key Points:
- We report significant increases in precipitation minus runoff in two deciduous forested watersheds
- The non-stationary hydrologic behavior is closely correlated with growing season length, as determined from independent remote sensing data
- These long-term and interannual hydrologic nonstationary behavior were attributed primarily to minimum temperature regimes

Supporting Information:
- Figure S1

Correspondence to:
T. Hwang,
taehee@indiana.edu

Citation:
Hwang, T., Martin, K. L., Vose, J. M., Wear, D., Miles, B., Kim, Y., & Band, L. E. (2018). Nonstationary hydrologic behavior in forested watersheds is mediated by climate-induced changes in growing season length and subsequent vegetation growth. *Water Resources Research*, *54*, 5359–5375. https://doi.org/10.1029/2017WR022279

Received 29 NOV 2017
Accepted 4 MAY 2018
Accepted article online 14 MAY 2018
Published online 16 AUG 2018

Nonstationary Hydrologic Behavior in Forested Watersheds Is Mediated by Climate-Induced Changes in Growing Season Length and Subsequent Vegetation Growth

Taehee Hwang[1], Katherine L. Martin[2,3], James M. Vose[3], David Wear[3], Brian Miles[4], Yuri Kim[1], and Lawrence E. Band[4,5]

[1]Department of Geography, Indiana University Bloomington, Bloomington, IN, USA, [2]Department of Forestry and Environmental Resources, North Carolina State University, Raleigh, NC, USA, [3]Center for Integrated Forest Science, Southern Research Station, USDA Forest Service, North Carolina State University, Raleigh, NC, USA, [4]Institute for the Environment, University of North Carolina at Chapel Hill, Chapel Hill, NC, USA, [5]Department of Geography, University of North Carolina at Chapel Hill, Chapel Hill, NC, USA

Abstract Forested watersheds provide important ecosystem services through the provision of high quality freshwater, mitigation of floods, and maintenance of base flows. How alteration of these services under ongoing climate change is mediated by vegetation dynamics is not fully understood. Combining independent remote sensing based vegetation information and distributed hydrological modeling, we investigated the impact of climate-induced vegetation dynamics on long-term non-stationary hydrologic behavior in two forested watersheds in the southern Appalachians. We found significant increases in precipitation-runoff deficit (defined as annual precipitation minus annual runoff), equivalent to annual evapotranspiration plus storage changes, over the last three decades. This non-stationary hydrologic behavior was significantly correlated with long-term and interannual changes in growing season length and subsequent vegetation growth. These patterns in vegetation phenology were attributed primarily to minimum temperature regimes, which showed steeper and more consistent increases than temperature maxima. Using a distributed modeling framework, we also found that the long-term non-stationary hydrologic behavior could not be simulated unless full vegetation dynamics, including vegetation phenology and long-term growth, were incorporated into the model. Incorporating seasonal vegetation dynamics also led to the improved simulation in streamflow dynamics, while its effect spread out through the following dormant seasons. Our study indicates that non-stationary hydrologic behavior has been closely mediated by long-term seasonal and structural forest canopy interaction with climate variables rather than directly driven by climatic variables. This study emphasizes the importance of understanding the ecosystem responses to ongoing climate change for predictions of future freshwater regimes.

1. Introduction

Forest watersheds provide valuable ecosystem services in the quantity and quality of freshwater resources in streamflow, dependent on the balance between precipitation (P) and evapotranspiration (ET). In the southern United States, forest ET represents a major terrestrial water loss to the atmosphere (see Table 2 in (Vose et al., 2015)), which is mainly attributed to interception and transpiration in closed canopied watersheds (Ford et al., 2007; Oishi et al., 2010; Wilson et al., 2001). Interception is a function of surface area of all aboveground structures (i.e., leaves, branches, stems, and forest litter etc.), which is determined primarily by aboveground biomass, disturbance, and successional processes over longer time scales (Ford et al., 2011). Leaf surface area and its seasonal dynamics (phenology) are major drivers of productivity (e.g., Barr et al., 2004; Delpierre et al., 2017; Keenan et al., 2014; Richardson et al., 2010) and transpiration (Wang et al., 2014); however, for a given leaf area, changes in species composition can also affect transpiration and subsequent water yield (Caldwell et al., 2016). Therefore, with a given set of atmospheric forcing variables, vegetation water use and resulting freshwater yield in forested watersheds are mediated by long-term structural and short-term physiological responses of vegetation, such as leaf area index and growing season length, as well as species-specific characteristics that regulate individual tree water use. In this sense, vegetation

patterns in space and time can therefore provide a 'gateway into underlying water balance' (Sivapalan, 2006) partitioning between terrestrial water loss and surface/subsurface drainage flow.

Analyses of long-term streamflow data from forested watersheds often suggest that streamflow trends are indicative of the interacting effects of successional processes, altered phenology, and changing water use efficiency (e.g., Caldwell et al., 2016). Despite the clear linkage between vegetation dynamics and associated hydrologic processes (Huntington, 2004; Huntington & Billmire, 2014), most studies have examined long-term hydrologic records or have used modeling approaches under steady-state canopy assumption (Milly et al., 2007); few studies have incorporated observed seasonal vegetation dynamics that adjust to changing climate as a major water balance control. Assuming steady-state vegetation conditions is no longer reasonable, as warmer temperatures have led to earlier green-up, delayed senescence, and longer growing seasons (e.g., Gunderson et al., 2012) and elevated CO_2 also has the potential to alter stomatal function and water use efficiency (e.g., Novick et al., 2015). This indicates a critical knowledge gap in our understanding of the combined effects of vegetation dynamics and climate change on hydrologic processes. In order to accurately predict ET and associated hydrologic processes such as streamflow and groundwater recharge, long-term analyses or model projections must account for short- to long-term vegetation stomatal and structural dynamics.

Vegetation phenology and subsequent growing season length (GSL) are regarded as key ecosystem responses to changing climate (e.g., Menzel et al., 2006). There have been many efforts to better represent vegetation phenology in terrestrial ecosystem and global circulation models (e.g., Kang et al., 2007; Richardson et al., 2012) to improve the representation of vegetation feedbacks and controls on photosynthesis, respiration, transpiration, and surface energy balances. However, phenological response has not been incorporated into watershed models as a major driver of streamflow non-stationarity although a few studies have examined the link (Puma et al., 2013; White et al., 1999). Long-term global satellite data (e.g., Advanced Very High Resolution Radiometer) provide an opportunity to estimate multi-decadal phenological shifts and vegetation dynamics, including leaf area and growing season length, at a medium spatial resolution. Using these global satellite data, many studies reported that the patterns in vegetation seasonality and duration have been very variable and complex globally since the early 1980s (e.g., Jeong et al., 2011).

Despite the importance of long-term vegetation dynamics in regulating hydrological processes, few studies have related watershed-scale hydrologic behavior to emergent long-term vegetation dynamics from global satellite products, mainly because they were often complicated by parallel land use and land cover (LULC) changes. For example, Czikowsk and Fitzjarrald (2004) used seasonal precipitation and runoff deficit to assess long-term shifts in green-up phenology in New England. Brooks et al. (2011) and Voepel et al. (2011) also showed how remotely sensed vegetation information from MODIS global satellite products was related to catchment-scale hydrologic partitioning across different climate regions. Recently, Creed et al. (2015) showed there has been significant intensification of the hydrological cycle in northern deciduous forests, indicated by more frequent droughts and high flow periods. This phenomenon was driven by a mismatch between phenological and hydrological processes, often referred as 'widening vernal and autumnal windows'. Understanding how hydrologic behavior responds to emergent vegetation dynamics is critical for providing insight into future freshwater availability under ongoing climate change.

In this study, we hypothesize that hydrologic regime changes under ongoing climate change are dependent on long-term structural and seasonal vegetation dynamics, including leaf area and growing season length, in forested headwater catchments. The dynamic vegetation changes provide non-stationary components of watershed hydrology, which need to be accounted for to understand long-term and interannual runoff dynamics. To examine the dominant controls on non-stationary hydrologic behavior, (1) we quantified the relationship between interannual/long-term non-stationary hydrologic behavior and remotely sensed vegetation dynamics in two forested headwater catchments in the southern Appalachians, and (2) examined whether the emergent long-term non-stationary hydrologic behavior could be simulated with and without detailed vegetation dynamics in a distributed hydrological modeling framework.

2. Methods and Materials

2.1. Study Sites

The study watersheds are located within the upper Yadkin basin in North Carolina; the Yadkin River at Patterson (USGS ID: 02111000; elevation range 360–1125 m and area 74.6 km^2) and the Elk Creek at Elkville

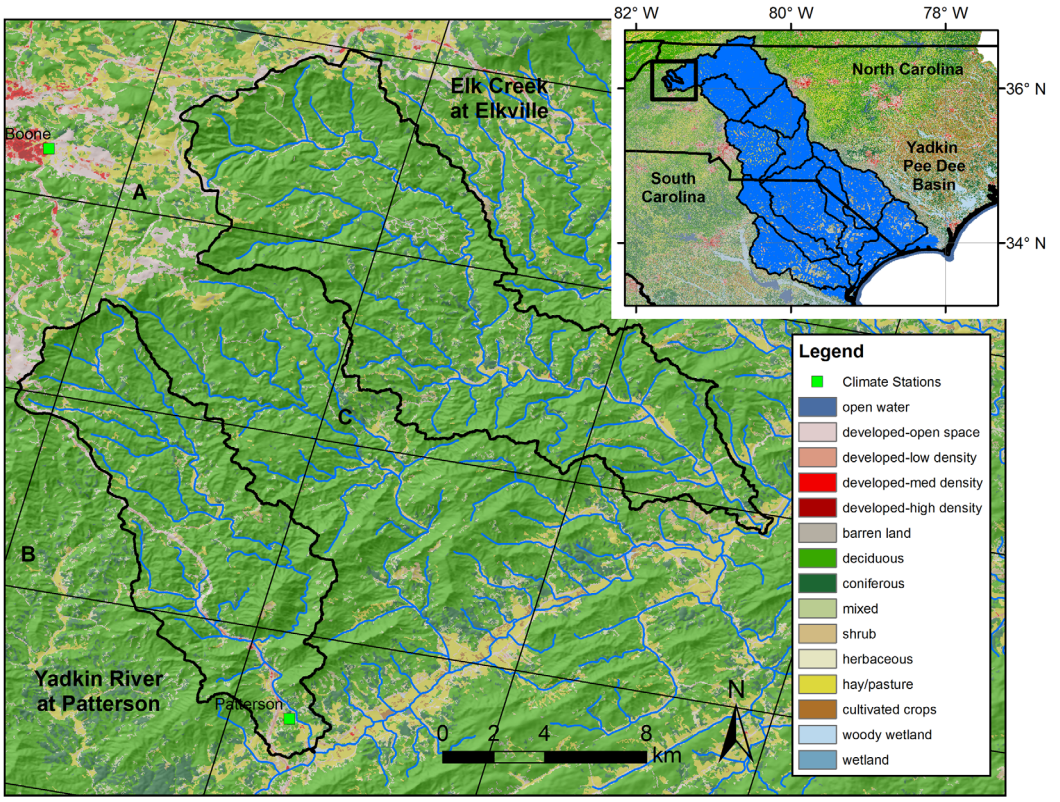

Figure 1. Study site: two forested study watersheds at the upper Yadkin basin (inset) in North Carolina, USA (Elk creek at Elkville – right, Yadkin river at Patterson – left). Detailed land use and land cover information is available in Table S2. Grids with letters (A/B/C) denote the GIMMS (Global Inventory Modeling and Mapping Studies) NDVI3g (third generation normalized difference vegetation index) data pixels used in this study.

(USGS ID: 02111180; elevation range 330–1240 m and area 131.8 km^2), referred to as 'Patterson' and 'Elk' hence (Figure 1). Long-term stream discharge records for these two watersheds are available from 1939 and 1956, with observed annual water yields of 582 (± 234) mm and 618 (± 253) mm for Patterson and Elk watersheds, respectively. In general, the two study watersheds showed very similar precipitation and streamflow patterns. Monthly mean temperature ranges from 2.2°C in January to 23.8°C in July. Annual precipitation is 1,221 mm at the base of the Patterson watershed (330 m elevation). Precipitation was relatively evenly distributed throughout the year with greater interannual variability during the summer.

LULC information from the 2006 National Land Cover Dataset (NLCD) indicates that both study watersheds are composed of about 90% forests (mostly deciduous), 5% hay/pasture and other land uses (Figure 1 and supporting information Table S2). We also found no significant changes in LULC and no permanent snowpack at the study watersheds from visual inspection of historic Landsat TM (Thematic Mapper) imagery since 1984. Both study watersheds are included in the Southern Crystalline Ridges and Mountains subsection of the Blue Ridge Mountain ecoregion, characterized by high relief and acidic, well-drained loamy soils underlain by Precambrian-age igneous and high-grade metamorphic rock (Griffith, 2002). Forest Inventory and Analysis (FIA) data from Watauga, Caldwell and Wilkes counties suggest *Liriodendron tulipifera* (tulip-poplar), *Quercus prinus* (chestnut oak), *Pinus echinata* (eastern white pine), *Acer rubrum* (red maple), *Fagus grandifolia* (American beech), *Q. alba* (white oak) and *Q. coccinea* (scarlet oak) are the most abundant overstory species in the study watersheds (Griffith, 2002). These two medium-scale forested watersheds provide us an opportunity to examine how forests dynamics affect hydrologic regime changes, estimated from long-term remote sensing data at coarse spatial scale.

2.2. Climate Data Sets

The Patterson watershed contains a long-term (1898 to present) precipitation gauge (Patterson, NC Climate Station ID: 316602). Daily precipitation data from adjacent climate stations were also used to fill missing

data and to estimate orographic patterns and basin-wide representative values assuming a simple linear trend with elevation (supporting information Table S1 and Figure S1). To estimate the long-term changes in orographic precipitation reported in this region (Burt et al., 2018), we used scatterplots of total monthly precipitation between low- and high-elevation climate stations (Patterson – 387 m; Grandfather Mtn – 1,615 m) with three-year moving windows (supporting information Figure S2). Due to frequent missing data at the high elevation station, we only used the months with full data records. We found a significant decreasing trend in their regression slopes during the study period (supporting information Figure S3), incorporated into both empirical and modeling approach in this study.

Daily maximum and minimum temperature data from the closest climate station along the mountain range (W Kerr Scott Reservoir; NC Climate Station ID 319555) were used in this study, as well as daily precipitation data. This climate station is located approximately 20 km to the east of the study watersheds. Using the MT-Clim model algorithm (Running et al., 1987), daily climate data from the base climate station were extrapolated with spatial topographic characteristics, including elevation, aspect, and slope. Environmental and dew-point temperature lapse rates were also estimated from scatter plots of daily temperatures between the climate stations. Daily atmospheric CO_2 levels were used in the model, interpolated from monthly data from the Mauna Loa station (Hawaii, USA) (http://cdiac.ornl.gov/ftp/trends/co2/maunaloa.co2). To examine the long-term trends in temperature regimes, we used a linear regression analysis to calculate changes in daily maximum and minimum temperatures. We applied these analyses seasonally (winter, spring, summer, and autumn) to examine divergent trends in temperature regimes between growing and dormant seasons, and between maximum and minimum temperatures. Details of the climate data used in this study were summarized in supporting information Table S1.

Water balance approach

The water balance at the watershed scale can be written as:

$$P - Q = ET + \Delta S \tag{1}$$

where P is precipitation, Q is runoff, ET is evapotranspiration, and ΔS is the change in soil water storage. In this study, we used the concept of 'vegetation year' in the mass balance calculation, suggested by Troch et al. (2009). Vegetation year represents the period from the beginning of growing season to the end of following the dormant season (supporting information Figure S4). Note that we used a June-May vegetation year in this study because leaf out would not be complete in May especially at high elevations in the study watersheds (supporting information Table S2) (Hwang et al., 2014). In deciduous forests without permanent snowpack, precipitation during dormant season recharges storage depletion (ΔS) (assuming low ET) accumulated during the growing season. We calculated P minus Q values from Eq. 1 (called 'P-Q deficit' hereafter) each year from long-term precipitation and streamflow records. Although the water balance equation provides a simple way to estimate the watershed-scale ET assuming negligible storage changes, the P-Q deficit value in the current vegetation year may still include transient effects of storage depletion from the previous vegetation year, as ΔS in eq. 1.

2.3. Vegetation Information From Landsat Thematic Mapper (TM) Images

We analyzed fourteen Landsat TM images during the peak growing season (June to August) for the study watersheds from 1986 to 2008 (supporting information Figure S5). Landsat TM, initially launched in 1984, provides a nearly three-decade multispectral satellite record from one satellite sensor system. All images were provided with a standard level-1 terrain correction and checked manually for cloud contamination within the two watershed boundaries. A modified dark object subtraction (DOS) method with the effect of Rayleigh scattering was applied to correct atmospheric effects on surface reflectance (Song et al., 2001). We calculated the normalized difference vegetation index (NDVI) to estimate the changes in vegetation patterns at fine resolution (30 m) over the study period. NDVI is a normalized ratio between surface reflectance of red and near infrared bands. NDVI provides consistent spatial and temporal criteria for vegetation conditions that linearly responds to the absorption of photosynthetically active radiation, thus the ecosystem energy input and subsequent latent heat flux (Song et al., 2013). A maximum leaf area index (LAI) map was derived from the average NDVI values from three cloud-free summer images (July 30, 1986, June 6, 1993, and August 11, 2008). The NDVI-LAI relationship was derived from a previous study in southern Appalachian hardwood forest (Hwang et al., 2009), using optical and field measurements. These LAI values range from 3

to 5 in forest pixels (Figure 3c), which is within the range reported for other forested watersheds in the region (Bolstad et al., 2001). Due to frequent cloud contamination and uncertainty in preprocessing in the mountainous terrain, we used nine absolutely cloud-free images to calculate the mean and standard deviations of NDVI and LAI values within the two study watersheds to compare with the simulated ones. The other five TM images were used to visually examine major forest cover changes at the study watersheds, which were mostly contaminated by spotty clouds.

2.4. Long-Term Vegetation Phenology From GIMMS NDVI3g

We used the bi-monthly 8-km Global Inventory Modeling and Mapping Studies (GIMMS) NDVI3g (third generation normalized difference vegetation index) data set to extract long-term phenological records (1982–2013) for the study site (Fensholt & Proud, 2012) (https://nex.nasa.gov/nex/projects/1349/). The GIMMS NDVI3g product was derived from Advanced Very High Resolution Radiometer (AVHRR) imagery by reducing the variations due to sensor calibration, view geometry, and volcanic effect (Tucker et al., 2005). We extract the time series of NDVI values from three GIMMS NDVI3g pixels, majorities of which are located within the boundaries of the study watersheds (Figure 1). Post-filtering and fitting techniques were applied to multi-year NDVI data sets to get the mid-point NDVI value between maximum and minimum values (Hwang et al., 2011a), where the long-term phenological records were extracted from the intersections between mid-NDVI values (horizontal lines) and time-series NDVI lines as day of year (White et al., 2009) (Figure 2). Growing season length (GSL) is defined as the days between these two intersections, as green-up and senescence each year. In a previous study, we demonstrated that the estimated long-term vegetation phenology in the southern Appalachians was closely correlated with ground observations and MODIS-derived vegetation phenology (Hwang et al., 2014). We also calculated the average NDVI values during the peak growing season (June to August) from the GIMMS NDVI3g values. For long-term trend analysis for the

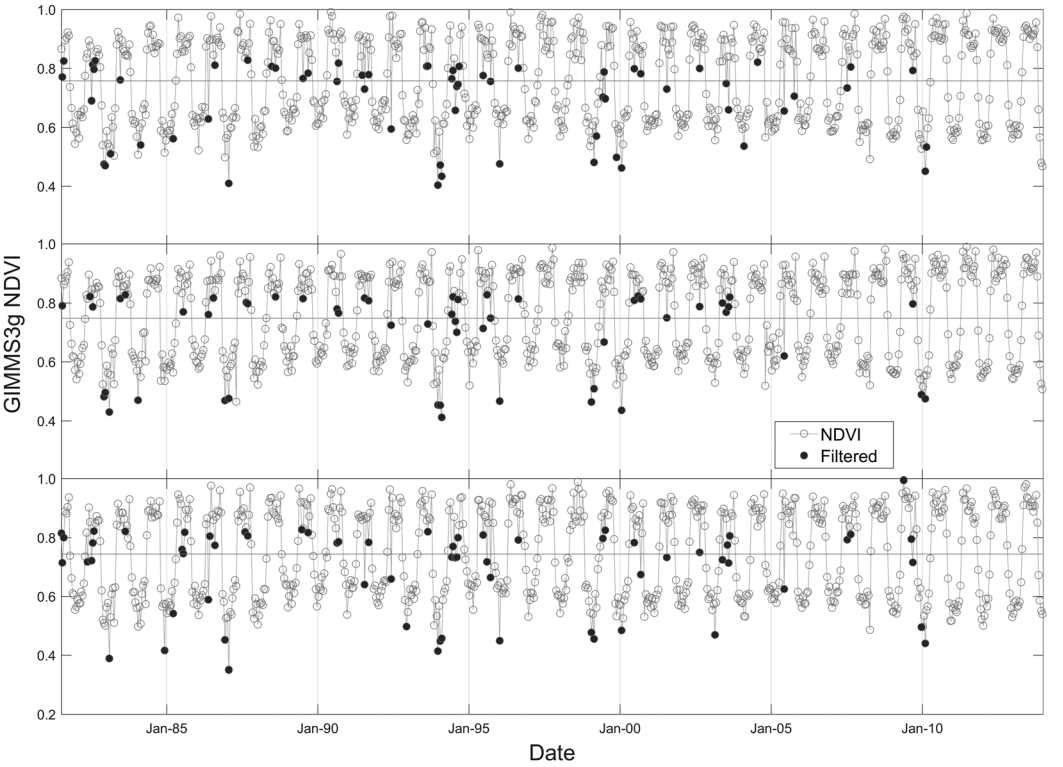

Figure 2. The time series of GIMMS (Global Inventory Modeling and Mapping Studies) normalized difference vegetation index (NDVI3g) values (open symbols) at three 8-km pixels in the study site. Black dots represent filtered values by an outlier exclusion method (*Hwang et al.*, 2011a). Horizontal lines are mid-point NDVI values for each pixel between fitted maximum and minimum NDVI values as a function of day of year (DOY). Green-up and senescence timing (DOY) were determined from the intersections between the horizontal lines and time-series NDVI lines, and growing season length (GSL – days) is defined as the days between green-up and senescence each year. The plots with DOY are available in Figure S4.

phenology and mean NDVI data, we performed both the Mann-Kendall and the Spearman's rho tests with the null hypothesis of trend absence in all time-series data.

To examine the dominant controls of temperature regimes on vegetation seasonality, we compared the timing of green-up and senescence for each year with the daily maximum/minimum temperatures from the closest climate station (W Kerr Scott Reservoir; supporting information Table S1). We calculate daily mean temperatures in April for green-up and from September to mid-October for senescence because our previous studies showed that the length of the transition periods (i.e. green-up to maturity onsets and senescence to dormancy onsets) were usually longer for senescence than green-up (Hwang et al., 2011a). We also compared the timing of green-up and senescence with the number of days when daily minimum temperatures were above freezing ($> 0°C$) for green-up and close to freezing ($< 5°C$) for senescence. These metrics were calculated from the periods between mid-February and April for green-up, and between August and mid-October for senescence. Note that these threshold-based metrics represent risk of frost damage to vegetation (Chuine, 2010), also a critical measure for modeling vegetation phenology (e.g., Vitasse et al., 2011).

2.5. Distributed Ecohydrological Model (RHESSys)

RHESSys (Regional Hydro-Ecological Simulation System) is a GIS-based, eco-hydrological modeling framework designed to simulate carbon, water, and nutrient cycling in complex terrain (Band et al., 1993; Tague & Band, 2004). RHESSys couples a patch-scale ecosystem model developed from BIOME-BGC (Running & Hunt, 1993) and CENTURY (Parton et al., 1996) with a distributed hydrologic model that routes water and solutes through topographically defined flow networks connecting patch and hillslope hydrology to regional stream network. The routing algorithm in the model was modified from the Distributed Hydrology Soil Vegetation Model (DHSVM) (Wigmosta et al., 1994), assuming fixed drainage along topographic gradients for both surface and saturated subsurface flows. RHESSys uses the Penman-Monteith equation for evapotranspiration, separately calculating transpiration for sunlit and shaded portions of the canopy (Tague & Band, 2004). The spatially gridded distributed structure of the model allows us to fully incorporate pixel-based remote sensing data at different spatial resolutions. RHESSys was applied to the study watersheds at a 30-m resolution, corresponding to the NLCD dataset.

The model was calibrated with seven key hydrological parameters: the decay rate of saturated hydraulic conductivity with soil depth (*m* for both vertical and lateral dimensions), the saturated hydraulic conductivity at soil surface (K_{sat0} for both dimensions), soil depth, and two conceptual groundwater storage parameters (*gw1* and *gw2*). The *gw1* parameter represents a percent amount of infiltration moving to deep groundwater stores, while the *gw2* parameter is a first-order rate constant from the store. Other ecophysiologic and soil parameterizations were based on detailed field observations in the southern Appalachians from previous studies (Hales et al., 2009; Hwang et al., 2009). More detailed descriptions regarding the related equations with these parameters are available in Tague and Band (2004).

Monte Carlo simulations were implemented 4,000 times for the period of October 2004 to September 2007 using the seven parameters randomly sampled within predefined ranges (supporting information Figure S6). Nash-Sutcliffe (N-S) efficiency of daily log streamflow data was used as an objective function to identify behavioral parameter sets (Nash & Sutcliffe, 1970), which emphasized low flows (rather than peaks) in calibration. We focused our calibration on low flows, which were more closely coupled with vegetation water use in this region (Hewlett & Hibbert, 1963). To include parameter uncertainty in model simulations, simulation sets above the 97.5% upper percentiles in model performance ($n = 100$) were selected as behavioral runs following the Generalized Likelihood Uncertainty Estimation (GLUE) methodology (Beven &Binley, 1992; Freer et al., 1996). Following calibration, the model was run from 1982 to 2013 with a two-year spin-up for all behavioral parameters sets, and 95% uncertainty boundaries in behavioral model runs were examined in further model simulations.

2.6. Model Simulation Schemes With Two Different Vegetation Dynamics

We hypothesized that emergent long-term non-stationary hydrologic behavior could not be simulated without incorporating detailed vegetation dynamics within our modeling framework. To test this hypothesis, the model was run with two different vegetation schemes, 'static' vs. 'dynamic' (Figure 3).

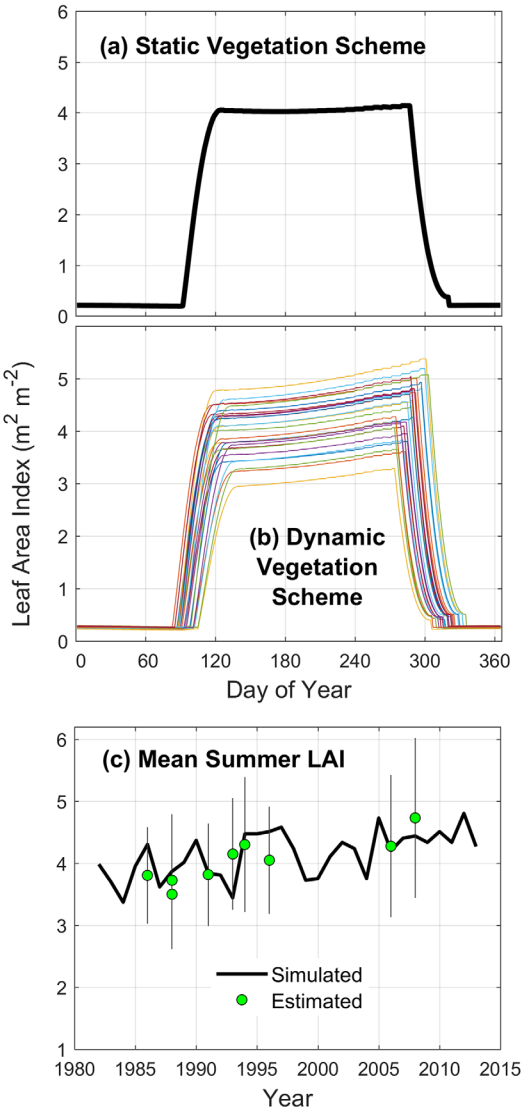

Figure 3. Basin-wide average leaf area index (LAI) dynamics under (a) static and (b) dynamic vegetation schemes during the study period (1982–2013), and (c) simulated mean summer LAI values. Points represent basin-average LAI values estimated from nine cloud-free Landsat images with their standard deviations (vertical bars). Dynamic vegetation scheme incorporates interannual variation in seasonal LAI, including green-up and senescence. Note that these seasonal LAI patterns imitate the seasonal normalized difference vegetation index (NDVI) patterns in the study watersheds (Figure S4). The model usually simulates high summer LAI values with longer growing season (especially earlier green-up) under the dynamic vegetation scheme. Note that the dynamic vegetation scheme is designed to simulate the 'lagged effect of earlier spring' in photosynthesis suggested by Richardson et al. (2010).

1. The first vegetation scheme used averaged seasonal LAI patterns without any interannual variation in maximum LAI and vegetation phenology (i.e. "static" vegetation scheme; Figure 3a). Under this scheme, the model used only spatial variation in maximum LAI values from three summer Landsat images, but without any year-to-year variation in LAI or phenology. Hence, the average timing of vegetation phenology from GIMMS NDVI3g (green-up, maturity, senescence, and dormancy onsets) and LAI were prescribed and held static for the model runs.
2. In the second scheme, the model was run with interannual variability of seasonal vegetation phenology and maximum LAI values (i.e. "dynamic" vegetation scheme; Figure 3b). The phenological timing was variable each year, and was prescribed from GIMMS NDVI3g data at the basin scale. The model simulates vegetation density (leaf area) from modeled carbon fixation based on light, water, and nutrient availability and allocation. The allocation process represents the partitioning of fixed carbon into major vegetation compartments (leaf, litter, fine root, live wood, and dead wood), including storage, utilization, and transport of carbohydrates (Hwang et al., 2009).

Under the dynamic vegetation scheme, the model usually produced higher summer LAI values with earlier green-up than the long-term average (Figure 3c), as well as a long-term increase in summer LAI values. The simulated LAI values are quite comparable with the estimated ones from the Landsat NDVI values (supporting information Figure S5) both interannual and long-term scales. Note that the dynamic vegetation scheme allowed us to simulate not only extended growing season during shoulder seasons, but also the 'lagged effect of earlier spring' (Figure 1 in *Richardson et al*., 2010) during peak growing season due to enhanced carbon uptake and subsequent high LAI within our modeling framework. More detailed descriptions regarding the growth-mode algorithm of RHESSys are available in Tague and Band (2004). Note that the combined use of GIMMS (coarse spatial resolution but frequent) and Landsat (fine spatial resolution but less frequent) imagery make it possible to take advantage of synergistic values of both image sets for application with the distributed ecohydrological modeling (Hwang et al., 2011b).

The model was calibrated under the static vegetation scheme assuming that behavioral soil hydrologic parameters are not changing. Then, we ran the RHESSys model with the vegetation schemes 1 (static) and 2 (dynamic) using the same calibrated hydrologic parameters and climate inputs, and examined simulated streamflow and ET in one of the study watersheds (Patterson) at seasonal and annual scales. These two simulation schemes were designed to disaggregate the net effect of vegetation dynamics on emergent non-stationary hydrologic behavior within our modeling framework. We are interested in how much vegetation dynamics, over and above the direct effects of interannual and long-term climate trends, can explain emergent hydrologic non-stationarity. Note that the simulation period in this study (1982–2013) was limited by the availability of the GIMMS NDVI3g data (Figure 2), required for the dynamic vegetation scheme.

Model performance for the streamflow was assessed using Nash-Sutcliffe efficiency values at daily and monthly scales and mean absolute errors (MAE) at monthly and yearly scales. The simulated differences between the two vegetation schemes were examined for all behavioral runs annually and seasonally to see

how extended growing season affect key hydrological fluxes (ET and streamflow). We also used a Pearson correlation matrix to examine inter-relationships among six key annual variables including mean daily maximum/minimum temperatures, P-Q deficit, GSL, and simulated annual ET under static and dynamic vegetation schemes. Finally, we calculated the residuals from the linear regressions of six annual variables with years to extract interannual variability signals by removing the common long-term trends, and applied correlation analyses to these detrended values.

3. Results

3.1. Divergence in Long-Term Temperature Trends

Overall, we found generally increasing trends in both daily maximum and minimum temperatures during the study period (Figure 4). Daily minimum temperatures consistently increased at 0.31-0.53°C per decade for all seasons, while warming trends in the daily maximum temperatures vary seasonally. When only the summer season (June-August) was considered, the daily maximum temperatures have increased 0.09°C per decade, while the daily minimum temperatures significantly increased 0.48°C per decade (Figure 4c; $p < 0.05$). More significant and steeper warming trends were found in daily minimum temperatures than maxima except for the winter (December-February). It is noteworthy that the rates of increase were much higher and more significant in daily minimum temperatures during the spring (March-May) and autumn (September-November) seasons, which are critical periods for green-up and senescence timing.

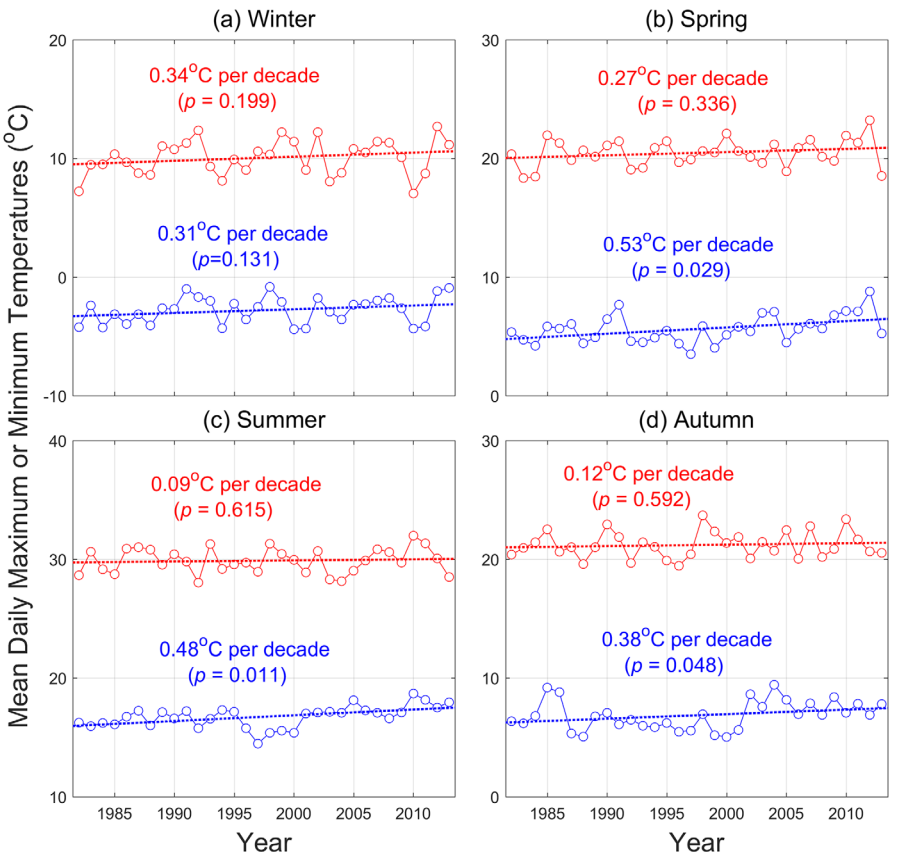

Figure 4. Temporal trends in mean daily maximum (red) and minimum (blue) temperatures (°C) for (a) winter (December-February), (b) spring (March-May), (c) summer (June-August), and (d) autumn (September-November) seasons. Temperature data were from the closest long-term climate stations (W Kerr Scott Reservoir – ID: 319555; Table 1). Note that the change rates of the temperatures were calculated from the linear regressions, while significance values were from a Mann-Kendall test.

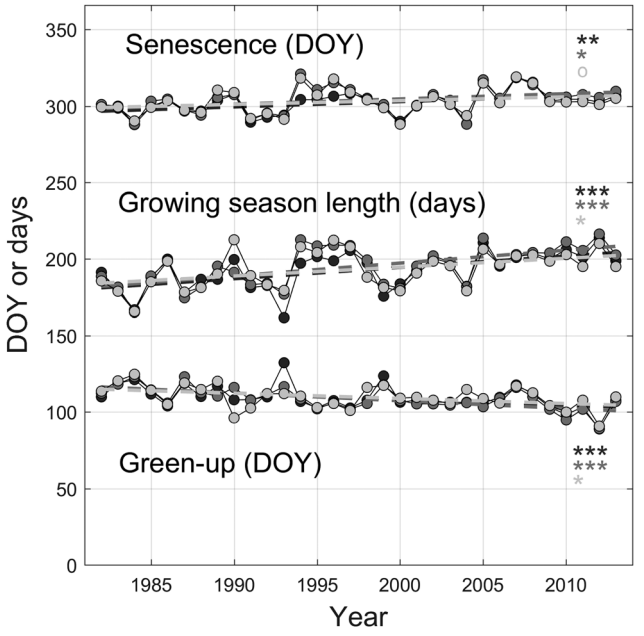

Figure 5. Leaf green-up (DOY), senescence (DOY), and growing season length (GSL – days) from the time-series of GIMMS NDVI data (Figure 2). GSL is defined as the number of days between leaf green-up and senescence each year. All three 8-km pixels (featured as different grey colors) show significant increasing trends in growing season length, reflected in earlier greenup and later senescence with time. $^{O}p < 0.1$, $^{*}p < 0.05$, $^{**}p < 0.01$ and $^{***}p < 0.005$.

3.2. Long-Term Trends in GSL, Vegetation Density and P-Q Deficit

From the time series of the GIMMS NDVI3g data, we found that growing seasons have significantly lengthened by about 23 days for all three GIMMS pixels ($p < 0.05$ for both trend analyses) during 31-year the study period (Figure 5), about 13 days earlier greenup and 10 days later senescence. This increase was reflected in the significant trends toward both earlier green-up and later senescence (Figure 5), where green-up advances were more consistent and statistically significant. Along with extended growing season, we found increases in the mean summer NDVI values from both GIMMS and Landsat TM images during the study period ($p < 0.01$ for all three GIMMS pixels; supporting information Figure S5), although we did not have enough cloud-free Landsat images for a statistical test. Note that the long-term increases in the GIMMS and Landsat NDVI values are consistent with our simulation of long-term summer LAI values under the dynamic vegetation scheme (Figure 3c).

The green-up and senescence timing each year was more significantly correlated with mean daily minimum temperatures in April ($r = -0.560$, $p < 0.005$; Figure 6a) and in September to mid-October ($r = 0.595$, $p < 0.001$; Figure 6d) than maxima (Figure 6b and e), respectively. This indicates that green-up has advanced by about 3.1 days while senescence is 2.8 days later per 1°C daily minimum temperature increase. The green-up timing also showed a more significant relationship with the number of days above freezing from mid-February ($r = -0.653$, $p < 0.001$; Figure 6c), while senescence had a more significant relationship with the number of days close to freezing from August ($r = 0.587$, $p < 0.001$; Figure 6f). This suggests that the extended growing season has been more closely correlated to long-term and interannual patterns in minimum rather than in maximum temperature regimes.

Long-term increases were also found in the P-Q deficit values during the study period (Figure 7a), about 181 and 217 mm (5.8 and 7.0 mm y^{-2}) for Patterson and Elk watersheds, respectively. These trends were significant in both trend analyses (Mann-Kendall and Spearman's rho tests), as well as the linear regressions ($p < 0.05$). This effectively indicates the long-term increases in watershed-scale ET for the study watersheds assuming negligible long-term storage changes. There were also significant correlations between the interannual P-Q deficit and GSL values for both original ($r = 0.537$, $p < 0.005$; Table 1) and detrended ones ($r = 0.436$, $p < 0.01$; Table 1). Linear regressions showed increases of 6.7 mm and 6.1 mm in the P-Q deficit values per unit increase of GSL for Patterson and Elk watersheds, respectively (inset in Figure 7). Note that we did not find any significant correlations between the P-Q deficit and annual hydrologic metrics, such as annual precipitation and streamflow (Figure 7b).

3.3. Hydrological Model Performance

The calibrated RHESSys models showed fairly good agreements between observed and simulated daily streamflow for the two study watersheds. For the three-year calibration period, the maximum Nash-Sutcliffe efficiency values for log-scale daily streamflow were 0.714 and 0.681 at Patterson and Elk watersheds, respectively (supporting information Figure S7). These efficiency measures were consistently lower for normal-scale daily streamflow data, which indicates potential shifts in peaks and uncertainty in daily orographic precipitation patterns in mountainous watersheds. For the long-term static vegetation simulation in the Patterson watershed, the Nash-Sutcliffe efficiency values were 0.566-0.661 and 0.608-0.713 for daily and monthly streamflow, respectively (Table 2 and supporting information Figure S8). Even without further calibrations, full dynamic vegetation simulation including both phenology and vegetation growth, showed improvements of approximately about 18.5% and 6.3% in median MAE values of annual and monthly streamflow, respectively (Table 2), as well as recognizable increases in Nash-Sutcliffe efficiency measures for both log daily and monthly streamflow. Note that the improvement in model performance was more

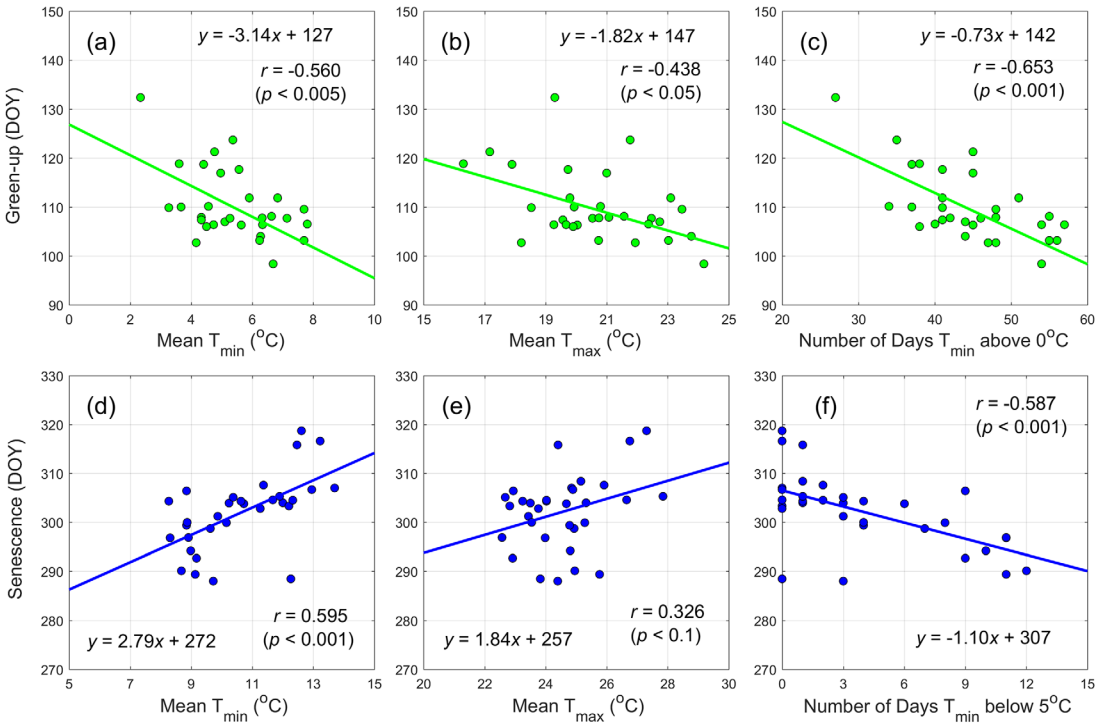

Figure 6. The sensitivity of green-up (upper panel – green; day of year) and senescence (lower panel – blue; day of year) to mean daily minimum (T_{min} - left column; °C), daily maximum (T_{max} - middle column; °C) temperatures, and number of days when T_{min} was above 0 for green-up or below 5 for senescence (right column; days) during the study period (1982–2013). The mean temperature values were calculated in April for green-up, while from September to mid-October for senescence. The number of days were calculated from the periods between mid-February to April for green-up and between August to mid-October for senescence.

prominent and significant with the performance measures at the longer time scales, especially in MAE values of annual streamflow.

The improved model performance was driven by the consistent increases in simulated LAI values (Figure 3c) and annual ET with longer growing seasons (Figure 8a) under the dynamic vegetation scheme (+2.8 mm per year; Figure 8b), compared to the simulation under the static vegetation scheme (+0.1 mm per year). This long-term increase in simulated ET is comparable with the simulated differences in annual ET and total runoff between the two vegetation schemes (+2.7 and −2.7 mm per year, respectively) (Figure 8b). This indicates that the model could not simulate the long-term increasing ET pattern without incorporating long-term seasonal and structural forest responses to climate change, longer growing season and subsequent higher LAI values.

3.4. Phenological Control on Key Hydrological Fluxes

The simulated annual ET values under the static vegetation scheme showed a moderately strong and significant correlation with mean daily maximum temperatures ($r = 0.573$; $p < 0.005$; Table 1). This possibly indicates atmospheric ET demands exerted a dominant control on interannual variation of simulated ET within the modeling framework. However, under the static vegetation scheme, we did not find a significant long-term trend (Figure 8b) or a correlation between simulated ET and the observed P-Q deficit (Table 1). In contrast, when full vegetation dynamics are incorporated (dynamic vegetation scheme), simulated ET showed stronger (and significant) correlations with both GSL ($r = 0.860$; $p < 0.005$; Table 1; Figure 8a) and P-Q deficit values ($r = 0.527$; $p < 0.005$; Table 1) with greater interannual variation (Figure 8b). Note that these correlation patterns remained the same even after the common trends were removed (Table 1). This indicates that the long-term and interannual non-stationary hydrologic behavior was driven, at least in part, by emergent vegetation dynamics, such as longer growing season and accompanying vegetation growth.

The seasonal comparison between the two vegetation schemes showed the increased ET with longer growing season not only during the shoulder seasons (spring and autumn) but also during the peak growing

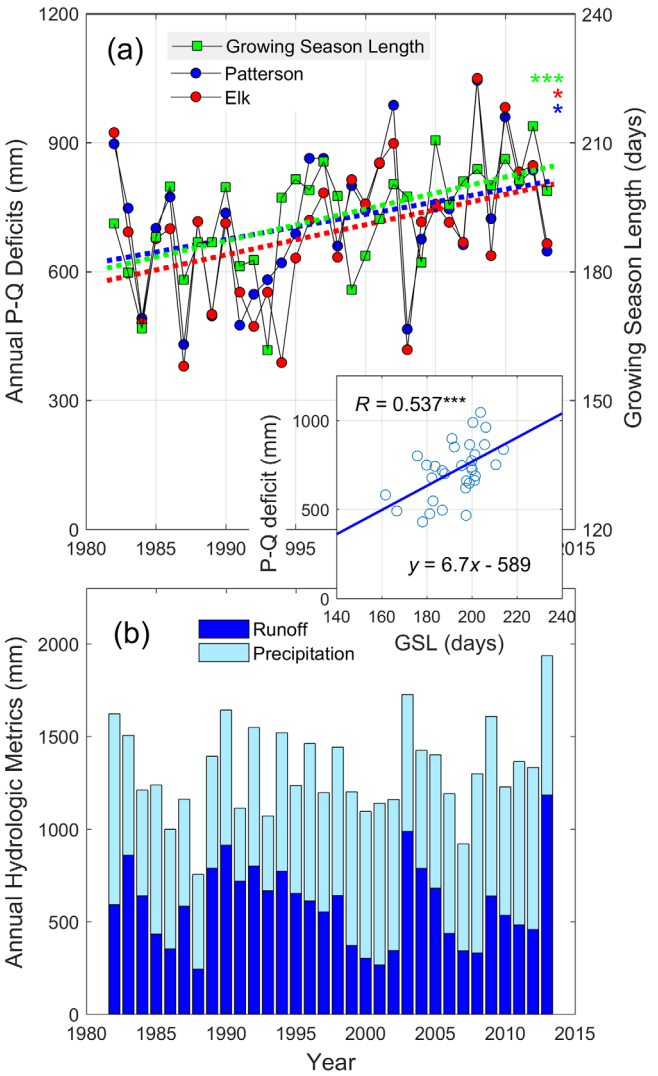

Figure 7. (a) Temporal patterns of annual precipitation minus runoff (P-Q deficit, mm) at Patterson (blue) and Elk (red) watersheds, and averaged growing season length (GSL, days – green; Figure 5) at the study watersheds. The inset is a scatter plot between the GSL and P-Q deficit values at Patterson watershed. All time-series data show significantly increasing trends, as well as a significant correlation between the detrended P-Q deficit and GSL values ($r = 0.462$, $p < 0.01$ – Patterson; Table 1). (b) Observed annual precipitation and runoff at Patterson watershed for a vegetation year (June to May). There is no significant trend in annual P and Q data. *P*: precipitation, *Q*: runoff. *$p < 0.05$, **$p < 0.01$, and ***$p < 0.005$.

season (June-August) due to high LAI values (Figure 9). Meanwhile, the effect of decreased streamflow due to the longer growing season spread out through the March to May period in the following years (Figure 9). However, the introduction of full vegetation dynamics did not completely explain the full range of long-term non-stationarity in the model (Figure 8b and supporting information Figure S9). In the both vegetation schemes, we still see strong autocorrelation patterns in the residuals of annual P-Q deficit especially during the period from 1989 to 1995 (supporting information Figure S9).

4. Discussion

4.1. Hydrologic Nonstationarity and Vegetation Phenology

We found that P-Q deficit values have increased significantly in the two forested watersheds during the last three decades, and were strongly correlated with long-term increase and interannual variability in growing season length and vegetation density (as indicated by independent remote sensing data). We attributed increases of growing season lengths primarily to daily minimum temperatures in spring and autumn, which showed steeper and more consistent increases than maximum daily temperatures. Within our ecohydrological modeling framework, we were able to simulate this long-term non-stationary hydrologic behavior (increasing ET) only when we included dynamic ecosystem responses to changing climate, such as increased leaf area and lengthened growing season. This suggests that the long-term increase in the P-Q deficit was at least partially attributed to increasing vegetation water use and interception (in the form of ET) in the study watersheds, as soil evaporation is typically a small fraction of total ET in closed canopied forests ((e.g.,10–15% of total ET) (Ford et al., 2007; Oishi et al., 2010).

In forested catchments, most throughfall infiltrates into the soil and is readily available for vegetation uptake, and Hortonian overland flow is rarely reported (Band et al., 2014). Therefore, vegetation usually has priority for the use of precipitation and infiltrated water as interception and transpiration up to a point where soil moisture exceeds ET demand (Brooks et al., 2010). In addition, despite relatively high annual rainfall, the southern Appalachians ecosystems are known to be moving toward more water-limited systems especially during the end of growing season due to high drainage efficiency and cumulative evaporative demand (Elliott et al., 2015; Hwang et al., 2014). Therefore, changing precipitation patterns (e.g., total amount and intensity) may have limited effects on runoff generation mechanisms in the forested watersheds, often rather featured by nonlinear runoff and recharge responses as a strong function of antecedent soil moisture condition (Detty & McGuire, 2010; McGuire & McDonnell, 2010; Scaife & Band, 2017). Instead, we suggest that vegetation water use, closely mediated by lengthened growing season and accompanying vegetation growth, has been a key source of hydrologic non-stationarity in the study watersheds at both decadal and seasonal time scales. Therefore, the changes in vegetation density and growing season length have been key drivers of precipitation and runoff relationships that determine freshwater availability in this region.

4.2. Growing Season Length as a Diagnostic for Hydrologic Regime Changes

Vegetation phenology exerts critical influence on canopy-level stomatal conductance and subsequent ET in temperate deciduous forests, especially during green-up periods (White et al., 1999; Wilson a& Baldocchi, 2000), when soil waters and other resources are abundant. Our modeling results also suggest strong

Table 1
Pearson Correlation Coefficients Among Six Key Annual Variables at Patterson Study Watershed: Mean Daily Maximum and Minimum Temperatures (T_{max} and T_{min}), Precipitation and Runoff Deficit (P-Q Deficit), Growing Season Length (GSL), and Simulated Median Evapotranspiration Under Static (ET_{static}) and Dynamic ($ET_{dynamic}$) vegetation Schemes (Figure 3)

	T_{max}	T_{min}	P-Q deficit	GSL	ET_{static}	$ET_{dynamic}$
T_{max}	1	0.329	0.132	−0.047	0.572***	0.268
T_{min}	0.269	1	−0.145	0.292	0.131	0.246
P-Q deficit	0.078	0.170	1	0.436**	0.174	0.429*
GSL	−0.004	0.587***	0.537***	1	−0.041	0.803***
ET_{static}	0.573***	0.118	0.181	−0.003	1	0.529***
$ET_{dynamic}$	0.260	0.522***	0.527***	0.860***	0.478**	1

[a]Note. Coefficient values in the upper right off-diagonal were from the detrended variables by removing the common long-term trends. Note that max and min temperatures were averaged during the whole growing season (May to September). *$p < 0.05$, **$p < 0.01$, and ***$p < 0.005$.

correlations between GSL and simulated ET at both seasonal and annual scales (Figures 8; and 9). Note that this was not just driven by the extended vegetation duration during the green-up and senescence periods, but also by the higher ET values during the peak growing season (Figure 9). In the deciduous forests of the eastern US, longer growing season (especially earlier green-up) often led to enhanced carbon uptake and higher LAI (e.g., Barr et al., 2004; Keenan et al., 2014; Richardson et al., 2010). Therefore, the emergent long-term correlations between GSL versus P-Q deficit and simulated ET were likely driven by a combination of extended growing season and the accompanying vegetation growth, as evident in the increase in summer NDVI values in our study site (supporting information Figure S5).

However, seasonal streamflow showed lagged responses to the incorporation of growing season variations through the early growing season of the following years (Figure 9). This suggests strong memory effect of growing season variations and subsequent ET on streamflow dynamics, mediated by changes in soil moisture storages (Nippgen et al., 2016; Scaife & Band, 2017). Nippgen et al. (2016) reported that the storage estimates from previous calendar years were strongly correlated to the relationship between annual precipitation and runoff in current years at Coweeta Hydrologic Laboratory, which indicated the strong memory effect of southern Appalachian watershed systems. This also suggests that vegetation dynamics and feedbacks increased the level of hydrologic non-stationarity in streamflow dynamics throughout the year, not just during the growing season. This might be a reason why several studies were not able to successfully separate phenological and meteorological controls on streamflow dynamics under different modeling frameworks in spite of their apparent link (Puma et al., 2013; White et al., 1999). This study would be the first study to incorporate vegetation phenology into watershed hydrology models as a major driver of long-term and seasonal hydrologic non-stationarity in forested watersheds. In this sense, we suggest that GSL would be an effective diagnostic for hydrologic regime changes under changing climate especially for deciduous forested catchments.

4.3. Vegetation Phenology Under Climate Change

Vegetation phenology is regarded as a sensitive indicator of ecosystem responses to climate change (Korner & Basler, 2010), strongly controlled by climate conditions during green-up and senescence periods (Estrella & Menzel, 2006; Hwang et al., 2011a; Richardson et al., 2010). Our results indicate that the study watersheds have experienced earlier green-up and delayed senescence with warming, consistent with the previous

Table 2
Model Performance Under Static and Dynamic Vegetation Schemes (Figure 3) at Patterson Watershed

Vegetation Schemes	NSE of log daily streamflow	NSE of log monthly streamflow	MAE of annual streamflow	MAE of monthly streamflow
Static	0.566-0.661 (0.619)	0.608-0.713 (0.671)	98.1–108.4 (103.1)	11.9–13.5 (12.8)
Dynamic	0.608-0.688 (0.651)	0.652-0.745 (0.708)	80.7–88.3 (84.0)	11.2–12.8 (12.0)

Note. Ranges represent the 95% bounds of behavioral runs for each vegetation scheme ($n = 100$), and their medians in parentheses. NSE: Nash-Sutcliffe efficiency, MAE: mean absolute error

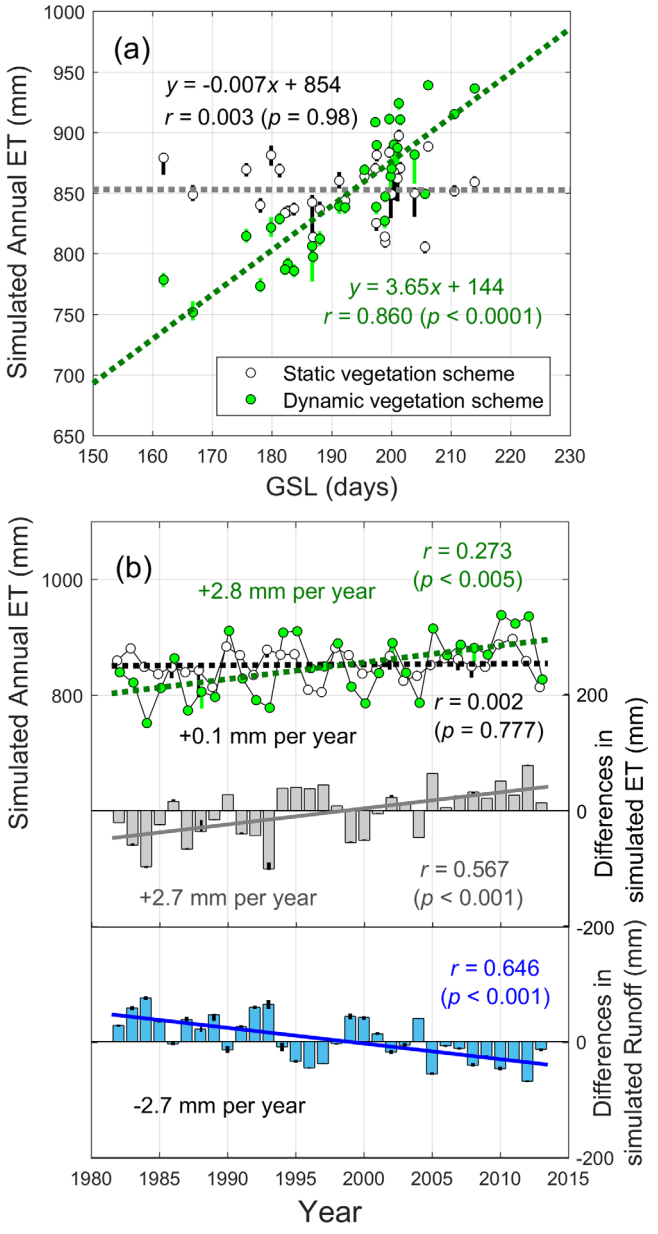

Figure 8. Scatterplots of growing season length (days) versus simulated differences in seasonal ET (upper panel; mm) and runoff (Q) (lower panel; mm) between two vegetation schemes ('dynamic - static'; Figure 3) during the study period (1982–2013). Vertical bars represent the simulated 95% uncertainty bounds from the behavioral runs ($n = 100$; Figure S6). Note that the periods of (d) December-February and (e) March-May represent the following calendar years. *$p < 0.05$, **$p < 0.01$, and ***$p < 0.005$.

local and global studies (Gunderson et al., 2012; Menzel et al., 2006). Vegetation phenology is considered more constrained by minimum rather than maximum temperature regimes in different ecosystems (e.g., Jarvis & Linder, 2000; Jolly et al., 2005; Robeson, 2002). This is related to a trade-off between maximizing carbon assimilation and reducing risk of frost damage (Chuine, 2010), as frost damage to shoots and buds is critical for its survival for most tree species (Kramer, 1995; Saxe et al., 2001).

Similar to our study, asymmetric increases between minimum and maximum temperatures, and between dormant and growing seasons, have been reported by other studies both locally and globally (Jones et al., 2012; Kim et al., 2013; Robeson, 2004; Thorne et al., 2016; Vose et al., 2005). It was also reported that global mean minimum temperature has been increasing twice (~0.2°C per decade) as fast as global maximum temperature (~0.1°C per decade) during the latter half of the 20th century (Folland et al., 2001). The nature of the changes in temperature regimes, affecting primarily minima rather than maxima, indicates a limited effect on vapor pressure deficit, and subsequent atmospherically-driven potential evaporation with warming (Roderick &Farquhar, 2002). This is consistent with long-term pan evaporation data in the southern Appalachians, which does not show a significant increasing trend during the study period (Hwang et al., 2012). This suggests that the emergent changes in hydrologic regime, such as increasing ET and decreasing runoff given precipitation, appear to have been mediated by vegetation dynamics rather than directly forced by climatic variables in the study watersheds, which suggests the strong negative feedback between vegetation function and watershed-scale water balance.

4.4. Additional Factors Contributing Long-Term Hydrologic Nonstationarity

Long-term non-stationarity behavior reflected by the increase in P-Q deficit ranged from 400 to 1,100 mm over the study period (Figure 7a), increasing by about 180 mm on average over the study period. However, the simulated annual ET ranged from about 750 to 940 mm over the same period with about less than 100 mm increase in annual simulated ET during the study period (Figure 8). This indicates that we were unable to simulate the full range of long-term non-stationary behavior even after including detailed vegetation dynamics in the model. There are several possible explanations for this.

First, we caution that the observed P-Q deficit values may not correctly reflect the ranges of actual ET in the study site, because annual soil storage changes are included in its calculation (ΔS in Eq. 1). As a result, P-Q deficit might include storage carry-over after wet years and groundwater recharges for the inherited deficit after dry years (Nippgen et al., 2016). Our modeling results also suggest that there is a significant amount of carry-over due to longer growing seasons from the previous years, however without any long-term trends in them (Figure 9 and supporting information Figure S10). Note that the long-term trend showed a few wet-dry cycles embedded within the full time domain, featured by autocorrelation patterns in annual runoff dynamics (Figure 7b). The study region experienced a severe drought in terms of both duration and absolute magnitude from the late 1985 through 1988 (Figure 7b). This prolonged drought was unprecedented; average annual precipitation was 1,033 mm during this period, 26% below normal. Therefore, the increase in the observed P-Q deficit after this drought period might include several-year recharges for possible deep groundwater storage depletion, also

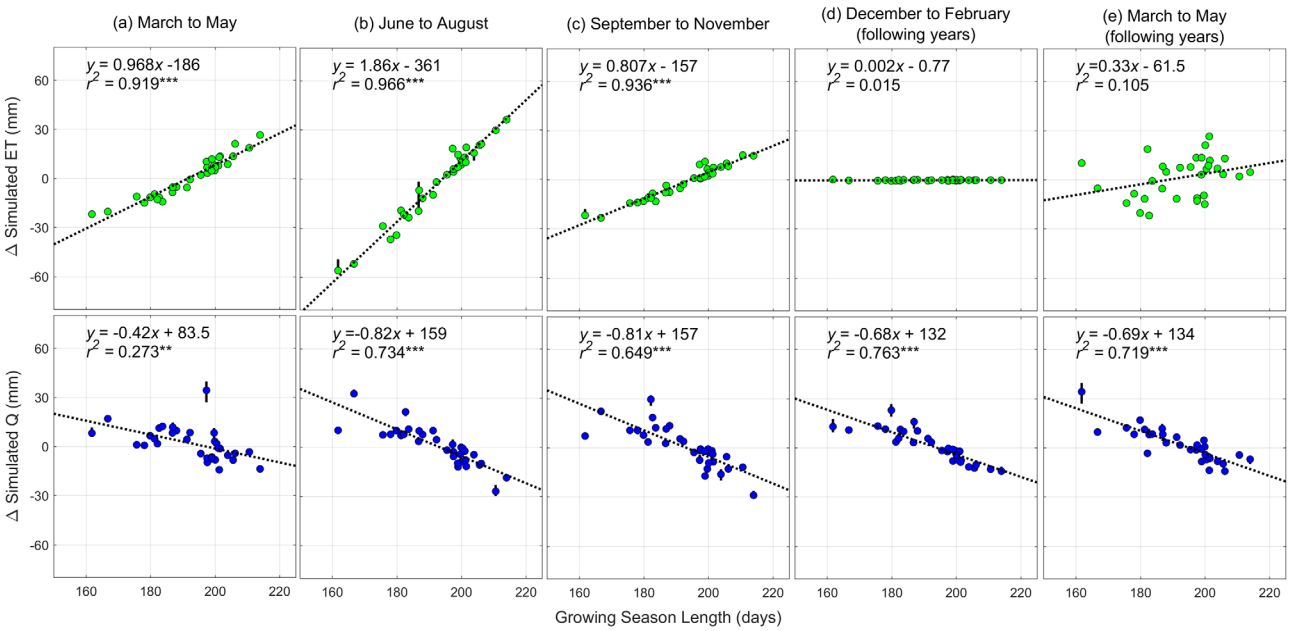

Figure 9. (a) Scatter plots of the simulated annual ET values (mm) under static (white) and dynamic (green) vegetation schemes (Figure 3) with growing season length (GSL – days; Figure 5) and, and (b) their long-term patterns and simulated differences in annual ET and runoff (mm) between two vegetation schemes. Vertical bars represent the simulated 95% uncertainty bounds from the behavioral runs ($n = 100$; Figure S6). Note that we were not able to simulate the long-term increase in annual ET (featured as a long-term increase in the P-Q deficit; Figure 7a) under the static vegetation scheme (white) within our modeling framework.

partially seen in our simulated storage changes at the end of May (supporting information Figure S10). Likewise, the autocorrelation patterns in the residuals of simulated annual P-Q deficit values during this period might be due to lack of detailed deep groundwater components in our model (supporting information Figure S9).

Second, ET is also greatly affected by the successional transitions in plant and tree species with different water use strategies and stomatal responses to soil water deficits (Caldwell et al., 2016; Vose & Elliott, 2016). In the southeastern U.S., reforestation under forest management has been governed by fire suppression policies (Wear & Greis, 2013), which has contributed to a transition from fire-tolerant oak (*Quercus*) species (especially *Q. alba*) to fire-sensitive species like maples (*Acer* spp.) and tulip poplar (*Liriodendron tulipifera*) (Abrams, 2003). Tulip poplar and red maple generally transpire more than *Carya* spp. (hickory) and oaks given topographic and climate conditions (Ford et al., 2011). In our modeling approach, we did not include potential transitions in tree species composition because we were limited by the data available for spatially distributed modeling over long-term scales. However, it is worthwhile to note that those two factors above (groundwater recharge and isohydric dominance due to fire suppression) can contribute only to the short- or long-term increase in the P-Q deficit, but not to the interannual variations.

5. Conclusions

In this study, we found that long-term and interannual non-stationary hydrologic behavior in the precipitation and runoff deficit was closely related to remotely sensed vegetation dynamics, including growing season length and vegetation density. Our work suggests that the minimum temperatures in spring and autumn are particularly important drivers in increasing growing season and subsequent vegetation growth, which have increased more rapidly than maximum temperatures during the last three decades. Using two schemes to represent vegetation dynamics within a detailed ecohydrologic model, we showed that both the interannual and long-term vegetation dynamics are necessary to capture short to long non-stationary hydrological behavior. We also suggest that observational and modeling approaches to detect and predict ecosystem water use and subsequent freshwater yield are very important to understand hydrologic non-stationarity under climate change, especially in forested watersheds.

While the forecasts of the future precipitation regime in the southern Appalachians are uncertain with respect to the mean, many studies indicate that hydroclimate variability will continue to increase (e.g., Ford et al., 2011; Seager et al., 2009). Approaches are needed to accurately project how vegetation dynamics and associated ecohydrological processes might respond to climate change, such as increased temperature and frequent drought conditions. The ongoing changes in forest composition and climate regime also highlight the need for future research to address how we can scale stomatal and other plant hydraulic regulation up to watershed-scale hydrologic behavior by linking ecosystem carbon uptake and water loss.

Acknowledgments
The research represented in this paper was supported by the USDA Forest Service, Southern Research Station (Agreement number: 14-JV-11330155-055). Any opinions, findings, conclusions, or recommendations expressed in the material are those of the authors and do not necessarily reflect the views of USDA Forest Service.

References

Abrams, M. D. (2003). Where has all the white oak gone? *BioScience*, *53*(10), 927–939.
Band, L. E., Patterson, P., Nemani, R., & Running, S. W. (1993). Forest ecosystem processes at the watershed scale: Incorporating hillslope hydrology. *Agricultural and Forest Meteorology*, *63*(1–2), 93–126.
Band, L. E., McDonnell, J. J., Duncan, J. M., Barros, A., Bejan, A., Burt, T., et al. (2014). Ecohydrological flow networks in the subsurface. *Ecohydrology*, *7*(4), 1073–1078.
Barr, A. G., Black, T. A., Hogg, E. H., Kljun, N., Morgenstern, K., & Nesic, Z. (2004). Inter-annual variability in the leaf area index of a boreal aspen-hazelnut forest in relation to net ecosystem production. *Agricultural and Forest Meteorology*, *126*(3–4), 237–255.
Beven, K., & Binley, A. (1992). The future of distributed models: Model calibration and uncertainty prediction. *Hydrological Processes*, *6*(3), 279–298.
Bolstad, P. V., Vose, J. M., & McNulty, S. G. (2001). Forest productivity, leaf area, and terrain in southern Appalachian deciduous forests. *Forest Science*, *47*(3), 419–427.
Brooks, J. R., Barnard, H. R., Coulombe, R., & McDonnell, J. J. (2010). Ecohydrologic separation of water between trees and streams in a Mediterranean climate. *Nature Geoscience*, *3*(2), 100–104.
Brooks, P. D., Troch, P. A., Durcik, M., Gallo, E., & Schlegel, M. (2011). Quantifying regional scale ecosystem response to changes in precipitation: Not all rain is created equal. *Water Resources Research*, *47*, W00J08. https://doi.org/10.1029/2010WR009762
Burt, T. P., Ford Miniat, C., Laseter, S. H., & Swank, W. T. (2018). Changing patterns of daily precipitation totals at the Coweeta Hydrologic Laboratory, North Carolina, USA. *International Journal of Climatology*, *38*(1), 94–104.
Caldwell, P. V., Miniat, C. F., Elliott, K. J., Swank, W. T., Brantley, S. T., & Laseter, S. H. (2016). Declining water yield from forested mountain watersheds in response to climate change and forest mesophication. *Global Change Biology*,
Chuine, I. (2010). Why does phenology drive species distribution? *Philosophical Transactions of the Royal Society B: Biological Sciences*, *365*(1555), 3149–3160.
Creed, I. F., Hwang, T., Lutz, B., & Way, D. (2015). Climate warming causes intensification of the hydrological cycle, resulting in changes to the vernal and autumnal windows in a northern temperate forest. *Hydrological Processes*, *29*(16), 3519–3534.
Czikowsk, M. J., & Fitzjarrald, D. R. (2004). Evidence of Seasonal Changes in Evapotranspiration in Eastern U.S. Hydrological Records. *Journal of Hydrometeorology*, *5*, 974–988.
Delpierre, N., Guillemot, J., Dufrêne, E., Cecchini, S., & Nicolas, M. (2017). Tree phenological ranks repeat from year to year and correlate with growth in temperate deciduous forests. *Agricultural and Forest Meteorology*, *234–235*, 1–10.
Detty, J. M., & McGuire, K. J. (2010). Topographic controls on shallow groundwater dynamics: Implications of hydrologic connectivity between hillslopes and riparian zones in a till mantled catchment. *Hydrological Processes*, *24*(16), 2222–2236.
Elliott, K. J., Miniat, C., Pederson, F. N., & Laseter, S. H. (2015). Forest tree growth response to hydroclimate variability in the southern Appalachians. *Global Change Biology*, 4627–4641.
Estrella, N., & Menzel, A. (2006). Responses of leaf colouring in four deciduous tree species to climate and weather in Germany. *Climate Research*, *32*, (3), 253–267.
Fensholt, R., & Proud, S. R. (2012). Evaluation of Earth Observation based global long term vegetation trends — Comparing GIMMS and MODIS global NDVI time series. *Remote Sensing of Environment*, *119*, 131–147.
Folland, C., Karl, Christy, T., Clarke, J., Gruza, R., Jouzel, G., Mann, J., Oerlemans, M., et al. (2001). The Scientific Basis. *Climate Change*, 99–181.
Ford, C. R., Hubbard, R. M., Kloeppel, B. D., & Vose, J. M. (2007). A comparison of sap flux-based evapotranspiration estimates with catchment-scale water balance. *Agricultural and Forest Meteorology*, *145*(3–4), 176–185.
Ford, C. R., Hubbard, R. M., & Vose, J. M. (2011). Quantifying structural and physiological controls on variation in canopy transpiration among planted pine and hardwood species in the southern Appalachians. *Ecohydrology*, *4*(2), 183–195.
Ford, C. R., Laseter, S. H., Swank, W. T., & Vose, J. M. (2011). Can forest management be used to sustain water-based ecosystem services in the face of climate change? *Ecological Applications*, *21*(6), 2049–2067.
Freer, J., Beven, K., & Ambroise, B. (1996). Bayesian estimation of uncertainty in runoff prediction and the value of data: An application of the GLUE approach. *Water Resources Research*, *32*(7), 2161–2173.
Griffith, G. E. (2002). *Ecoregions of North Carolina and South Carolina (color poster with map, descriptive text, summary tables, and photographs)*, Reston, VA: US Geological Survey.
Gunderson, C. A., Edwards, N. T., Walker, A. V., O'Hara, K. H., Campion, C. M., & Hanson, P. J. (2012). Forest phenology and a warmer climate - growing season extension in relation to climatic provenance. *Global Change Biology*, *18*(6), 2008–2025.
Hales, T. C., Ford, C. R., Hwang, T., Vose, J. M., & Band, L. E. (2009). Topographic and ecologic controls on root reinforcement. *Journal of Geophysical Research-*, *114*, F03013. https://doi.org/10.1029/2008JF001168
Hewlett, J. D., & Hibbert, A. R. (1963). Moisture and Energy Conditions within a Sloping Soil Mass during Drainage. *Journal of Geophysical Research*, *68*(4), 1081–1087.
Huntington, T. G. (2004). Climate change, growing season length, and transpiration: Plant response could alter hydrologic regime. *Plant Biology*, *6*(6), 651–653.
Huntington, T. G., & Billmire, M. (2014). Trends in precipitation, runoff, and evapotranspiration for rivers draining to the Gulf of Maine in the United States. *Journal of Hydrometeorology*, *15*(2), 726–743.
Hwang, T., Band, L. E., & Hales, T. C. (2009). Ecosystem processes at the watershed scale: Extending optimality theory from plot to catchment. *Water Resources Research*, *45*, W11425. https://doi.org/10.1029/2009WR007775

Hwang, T., Band, L. E., Miniat, C. F., Song, C., Bolstad, P. V., Vose, J. M., & Love, J. P. (2014). Divergent phenological response to hydroclimate variability in forested mountain watersheds. *Global Change Biology*, *20*(8), 2580–2595.
Hwang, T., Band, L. E., Vose, J. M., & Tague, C. (2012). Ecosystem processes at the watershed scale: Hydrologic vegetation gradient as an indicator for lateral hydrologic connectivity of headwater catchments. *Water Resources Research*, *48*, W06514. https://doi.org/10.1029/2011WR011301
Hwang, T., Song, C., Bolstad, P. V., & Band, L. E. (2011b). Downscaling real-time vegetation dynamics by fusing multi-temporal MODIS and Landsat NDVI in topographically complex terrain. *Remote Sensing of Environment*, *115*(10), 2499–2512.
Hwang, T., Song, C., Vose, J. M., & Band, L. E. (2011a). Topography-mediated controls on local vegetation phenology estimated from MODIS vegetation index. *Landscape Ecology*, *26*(4), 541–556.
Jarvis, P., & Linder, S. (2000). Constraints to growth of boreal forests. *Nature*, *405*(6789), 904–905.
Jeong, S.-J., Ho, C.-H., Gim, H.-J., & Brown, M. E. (2011). Phenology shifts at start vs. end of growing season in temperate vegetation over the Northern Hemisphere for the period 1982–2008. *Global Change Biology*, *17*(7), 2385–2399.
Jolly, W. M., Nemani, R., & Running, S. W. (2005). A generalized, bioclimatic index to predict foliar phenology in response to climate. *Global Change Biology*, *11*(4), 619–632.
Jones, J. A., Creed, I. F., Hatcher, K. L., Warren, R. J., Adams, M. B., Benson, M. H., et al,. (2012). Ecosystem processes and human influences regulate streamflow response to climate change at long-term ecological research sites. *BioScience*, *62*(4), 390–404.
Kang, H.-S., Xue, Y., & Collatz, G. J. (2007). Impact assessment of satellite-derived leaf area index datasets using a general circulation model. *Journal of Climate*, *20*(6), 993–1015.
Keenan, T. F., Gray, J., Friedl, M. A., Toomey, M., Bohrer, G., Hollinger, D. Y., et al. (2014). Net carbon uptake has increased through warming-induced changes in temperate forest phenology. *Nature Climate Change*, *4*(7), 598–604.
Kim, Y., Band, L. E., & Song, C. (2013). The Influence of Forest Regrowth on the Stream Discharge in the North Carolina Piedmont Watersheds. *JAWRA Journal of the American Water Resources Association*, *50*(1), 57–73.
Korner, C., & Basler, D. (2010). Phenology Under Global Warming. *Science*, *327*(5972), 1461–1462.
Kramer, K. (1995). Phenotypic Plasticity of the Phenology of 7 European Tree Species in Relation to Climatic Warming. *Plant Cell and Environment*, *18*(2), 93–104.
McGuire, K. J., & McDonnell, J. J. (2010). Hydrological connectivity of hillslopes and streams: Characteristic time scales and nonlinearities. *Water Resources Research*, *46*, W10543. https://doi.org/10.1029/2010WR009341
Menzel, A., Sparks, T. H., Estrella, N., Koch, E., Aasa, A., Ahas, R., et al. (2006). European phenological response to climate change matches the warming pattern. *Global Change Biology*, *12*(10), 1969–1976.
Milly, P., Julio, B., Malin, F., Robert, M., Zbigniew, W., Dennis, P., & Ronald, J. (2007). Stationarity is dead. *Ground Water News & Views*, *4*(1), 6–8.
Nash, J. E., & Sutcliffe, J. V. (1970). River flow forecasting through conceptual models part I — A discussion of principles. *Journal of Hydrology*, *10*(3), 282–290.
Nippgen, F., McGlynn, B. L., Emanuel, R. E., & Vose, J. M. (2016). Watershed memory at the Coweeta Hydrologic Laboratory: The effect of past precipitation and storage on hydrologic response. *Water Resources Research*, *52*. https://doi.org/10.1002/2015WR018196
Novick, K. A., Oishi, A. C., Ward, E. J., Siqueira, M. B., Juang, J. Y., & Stoy, P. C. (2015). On the difference in the net ecosystem exchange of CO2 between deciduous and evergreen forests in the southeastern United States. *Glob Chang Biol*, *21*(2), 827–842.
Oishi, A. C., Oren, R., Novick, K. A., Palmroth, S., & Katul, G. G. (2010). Interannual Invariability of Forest Evapotranspiration and Its Consequence to Water Flow Downstream. *Ecosystems*, *13*(3), 421–436.
Parton, W. J., Mosier, A. R., Ojima, D. S., Valentine, D. W., Schimel, D. S., Weier, K., & Kulmala, A. E. (1996). Generalized model for N-2 and N2O production from nitrification and denitrification. *Global Biogeochemical Cycles*, *10*(3), 401–412.
Puma, M. J., Koster, R. D., & Cook, B. I. (2013). Phenological versus meteorological controls on land-atmosphere water and carbon fluxes. *Journal of Geophysical Research: Biogeosciences*, *118*, 14–29. https://doi.org/10.1029/2012JG002088
Richardson, A. D., Black, T. A., Ciais, P., Delbart, N., Friedl, M. A., Gobron, N., et al. (2010). Influence of spring and autumn phenological transitions on forest ecosystem productivity. *Philosophical Transactions of the Royal Society B-Biological Sciences*, *365*(1555), 3227–3246.
Richardson, A. D., Anderson, R. S., Arain, M. A., Barr, A. G., Bohrer, G., Chen, G., et al. (2012). Terrestrial biosphere models need better representation of vegetation phenology: results from the North American Carbon Program Site Synthesis. *Global Change Biology*, *18*(2), 566–584.
Robeson, S. M. (2002). Increasing growing-season length in Illinois during the 20th century. *Climatic Change*, *52*(1), 2), 219–238.
Robeson, S. M. (2004). Trends in time-varying percentiles of daily minimum and maximum temperature over North America. *Geophysical Research Letters*, *31*, L04203. https://doi.org/10.1029/2003GL019019
Roderick, M. L., & Farquhar, G. D. (2002). The Cause of Decreased Pan Evaporation over the Past 50 Years. *Science*, *298*(5597), 1410–1411.
Running, S. W., & Hunt, E. R. (1993). Generalization of a forest ecosystem process model for other biomes, BIOME-BCG, and an application for global-scale models. In J. R. Ehleringer & C. B. Field (Eds.), *Scaling physiological processes: Leaf to globe* (pp. 141–158). San Diego, CA : Academic Press Inc.
Running, S. W., Nemani, R. R., & Hungerford, R. D. (1987). Extrapolation of synoptic meteorological data in mountainous terrain and its use for simulating forest evapotranspiration and photosynthesis. *Canadian Journal of Forest Research-Revue Canadienne De Recherche Forestiere*, *17*(6), 472–483.
Saxe, H., Cannell, M. G. R., Johnsen, Ø., Ryan, M. G., & Vourlitis, G. (2001). Tree and forest functioning in response to global warming. *New Phytologist*, *149*(3), 369–399.
Scaife, C. I., & Band, L. E. (2017). Nonstationarity in threshold response of stormflow in southern Appalachian headwater catchments. *Water Resources Research*, *53*, 6579–6596. https://doi.org/10.1002/2017WR020376
Seager, R., Tzanova, A., & Nakamura, J. (2009). Drought in the Southeastern United States: Causes, Variability over the Last Millennium, and the Potential for Future Hydroclimate Change. *Journal of Climate*, *22*(19), 5021–5045.
Sivapalan, M. (2006). Pattern, Process and Function: Elements of a Unified Theory of Hydrology at the Catchment Scale. In M. J. Anderson (Ed.), *Encyclopedia of Hydrological Sciences* (pp. 193-219). Hoboken, NJ: John Wiley & Sons, Ltd.
Song, C., Dannenberg, M. P., & Hwang, T. (2013). Optical remote sensing of terrestrial ecosystem primary productivity. *Progress in Physical Geography*, *37*, 834–854. https://doi.org/10.1177/0309133313507944
Song, C., Woodcock, C. E., Seto, K. C., Lenney, M. P., & Macomber, S. A. (2001). Classification and Change Detection Using Landsat TM Data: When and How to Correct Atmospheric Effects? *Remote Sensing of Environment*, *75*(2), 230–244.
Tague, C. L., & Band, L. E. (2004). RHESSys: Regional Hydro-Ecologic Simulation System–an object-oriented approach to spatially distributed modeling of carbon, water, and nutrient cycling. *Earth Interactions*, *8*(1), 1–42.

Thorne, P., Menne, M., Williams, C., Rennie, J., Lawrimore, J., Vose, R., et al. (2016). Reassessing changes in diurnal temperature range: A new data set and characterization of data biases. *Journal of Geophysical Research: Atmospheres*, *121*, 5115–5137. https://doi.org/10.1002/2015JD024583

Troch, P. A., Martinez, G. F., Pauwels, V., Durcik, M., Sivapalan, M., Harman, C., et al. (2009). Climate and vegetation water use efficiency at catchment scales. *Hydrological Processes*, *23*(16), 2409–2414.

Tucker, C. J., Pinzon, J. E., Brown, M. E., Slayback, D. A., Pak, E. W., Mahoney, R., et al. (2005). An extended AVHRR 8-km NDVI dataset compatible with MODIS and SPOT vegetation NDVI data. *International Journal of Remote Sensing*, *26*(20), 4485–4498.

Vitasse, Y., Francois, C., Delpierre, N., Dufrene, E., Kremer, A., Chuine, I., & Delzon, S. (2011). Assessing the effects of climate change on the phenology of European temperate trees. *Agricultural and Forest Meteorology*, *151*(7), 969–980.

Voepel, H., Ruddell, B., Schumer, R., Troch, P. A., Brooks, P. D., Neal, A., ET AL.(2011). Quantifying the role of climate and landscape characteristics on hydrologic partitioning and vegetation response. *Water Resources Research*, *47*, W00J09. https://doi.org/10.1029/2010WR009944

Vose, J. M., & Elliott, K. (2016). Oak, fire, and global change in the eastern USA: what might the future hold? *Fire Ecology*, *12*(2), 160–178.

Vose, J. M., Miniat, C. F., Sun, G., & Caldwell, P. V. (2015). Potential implications for expansion of freeze-tolerant eucalyptus plantations on water resources in the southern United States. *Forest Science*, *61*(3), 509–521.

Vose, R. S., Easterling, D. R., & Gleason, B. (2005). Maximum and minimum temperature trends for the globe: An update through 2004. *Geophysical Research Letters*, *32*, L23822. https://doi.org/10.1029/2005GL024379

Wang, L., Good, S. P., & Caylor, K. K. (2014). Global synthesis of vegetation control on evapotranspiration partitioning. *Geophysical Research Letters*, *41*, 6753–6757. https://doi.org/10.1002/2014GL061439

Wear, D. N., & Greis, J. G. (2013). Design of the Southern Forest Futures Project, *The Southern Forest Futures Project: Technical Report*.

White, M. A., Running, S. W., & Thornton, P. E. (1999). The impact of growing-season length variability on carbon assimilation and evapotranspiration over 88 years in the eastern US deciduous forest. *International Journal of Biometeorology*, *42*(3), 139–145.

White, M. A., Beurs, D., Kirsten, M., Didan, K., Inouye, D. W., Richardson, A. D., et al. (2009). Intercomparison, interpretation, and assessment of spring phenology in North America estimated from remote sensing for 1982–2006. *Global Change Biology*, *15*(10), 2335–2359.

Wigmosta, M. S., Vail, L. W., & Lettenmaier, D. P. (1994). A Distributed Hydrology-Vegetation Model for Complex Terrain. *Water Resources Research*, *30*(6), 1665–1679.

Wilson, K. B., & Baldocchi, D. D. (2000). Seasonal and interannual variability of energy fluxes over a broadleaved temperate deciduous forest in North America. *Agricultural and Forest Meteorology*, *100*(1), 565–578.

Wilson, K. B., Hanson, P. J., Mulholland, P. J., Baldocchi, D. D., & Wullschleger, S. D. (2001). A comparison of methods for determining forest evapotranspiration and its components: sap-flow, soil water budget, eddy covariance and catchment water balance. *Agricultural and forest Meteorology*, *106*(2), 153–168.